

Hubbard model on Semiclassical approximation in combination with an optimizer based on GPU technology

Hayun Park¹ and Hunpyo Lee¹

¹*Department of Liberal Studies, Kangwon National University, Samcheok, 25913, Republic of Korea*

(Dated: November 9, 2023)

We developed a semiclassical approximation method in combination with an adaptive moment estimation optimizer (SCA + ADAM) approach based on the PyTorch plus CUDA library on a the graphics processing unit (GPU). This method was employed to evaluate one-particle properties of the Hubbard model with long-range spatial correlations within an appropriate computing duration. The method was applied to the ionic Hubbard model on a two-dimensional square lattice with long-range spatial correlations. The computation time was evaluated as a function of the lattice size on the central processing unit and GPU. Herein, we also discuss the density of states and antiferromagnetic (AF) order parameter in the Hubbard model without the ionic potential and compare the results with those of the Hartree-Fock approximation. Finally, we present the one-particle properties and order parameter in charge density wave, AF metal and AF insulator of the ionic Hubbard model.

PACS numbers: 71.10.Fd, 71.27.+a, 71.30.+h

I. INTRODUCTION

Development of optimizers based on the graphics processing unit (GPU) technology has resulted in several breakthroughs in the field of artificial neural network. In addition, such optimizers have been extensively applied in various fields of computational science and economics involving optimization problems. Therefore, assessing the applicability of an optimizer to a GPU to solve interesting physical problems has garnered considerable attention in recent years.

The Hubbard model, which describes the competition between the kinetic energy of electrons and repulsive Coulomb potential energy of electrons, is one of the most popular and fundamental problems in physics [1]. The solutions of the Hubbard model are anticipated to reveal the origin of the high-temperature cuprate superconductivity, unconventional insulating behavior, and non-Fermi liquids appearing in two-dimensional (2D) electronic systems. Deriving an exact solution in the thermodynamic limit using the exact diagonalization (ED) method is limited, because the size of the Hamiltonian increases exponentially with an increase in the number of sites in a lattice [2, 3]. The unbiased quantum Monte Carlo (QMC) approach exhibits the infamous sign problem in the repulsive Fermionic Hubbard model [4, 5]. Moreover, the QMC method is restricted to moderately sized lattices owing to its computational burden. Therefore, despite numerous numerical efforts, development of novel numerical and theoretical methods for solving the Hubbard model continues to remain at the fore of research in this field [6–10].

A semiclassical approximation (SCA) approach is a well-established method for solving the Hubbard model [11, 12]. In the SCA, the onsite repulsive Hubbard interaction is decoupled into charge and spin fluctuations. A potential function with auxiliary fields is created via continuous Hubbard-Stratonovich transfor-

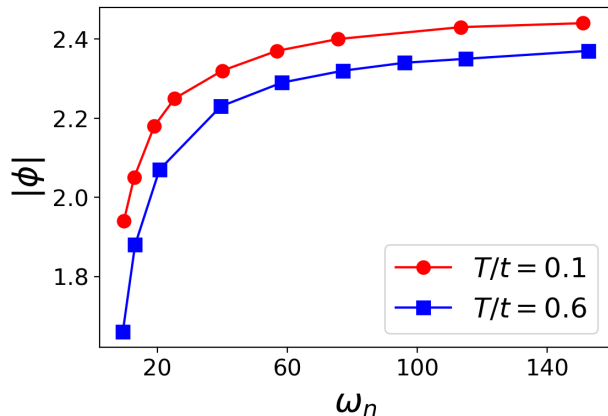


FIG. 1. (Color online) Antiferromagnetic order parameter $|\phi|$ as a function Matsubara frequency ω_n in the Hubbard model on half-filled two-dimension (2D) 20×20 square lattice at Hubbard interaction $U/t = 6.0$ for temperature $T/t = 0.1$ and 0.6 . ω_n is given as $\omega_n = (2n + 1)\pi T$, where n are integer numbers.

mation of the spin fluctuation term, and charge fluctuation is ignored. The number of auxiliary variables is equal to one of the sites on the lattice and increases with the increasing number of sites on the lattice. Determining the variables that minimize the potential energy is necessary in the SCA approach. However, the computational cost increases polynomially with an increase in the number of sites, thus impeding exploration of the Hubbard model with long-range spatial correlations. Accordingly, to date, the SCA has only been used in combination with the cluster dynamical mean field theory approach for a small-sized lattice system.

In this study, we developed an SCA integrated adaptive moment estimation optimizer (SCA+ADAM) approach based on the PyTorch plus CUDA library on a GPU. The auxiliary variables of the potential func-

tion created in the SCA were rapidly determined using a parallelized auto-gradient approach in the ADAM optimizer on the GPU [13]. Thus, the proposed integrated SCA+ADAM approach can be applied to a large Hubbard model with long-range spatial correlations. To evaluate the effectiveness of our SCA+ADAM approach, the approach was applied on the ionic Hubbard model of a half-filled 2D $L \times L$ square lattice, wherein electronic hopping, onsite periodic potential, and onsite repulsive Coulomb interactions induced a metallic state, band insulator (BI), and antiferromagnetic (AF) insulator, respectively. First, we examined the computational costs for various parameters on the central processing unit (CPU) and GPU. Next, we evaluated the density of states $\rho_\sigma(\omega)$ and AF order parameter ϕ of the Hubbard model without an onsite periodic potential. We also compared our SCA+ADAM results with those obtained using the Hartree-Fock method. Finally, the physical properties, phases and AF order parameter of the ionic Hubbard model were investigated.

The remainder of this paper is organized as follows: Section II describes the Hamiltonian of the ionic Hubbard model and formalism of the SCA approach. In Section III, computational cost and the results of $\rho_\sigma(\omega)$ and ϕ for both the pure and ionic Hubbard models are presented. Finally, the major conclusions drawn from the findings of this study are presented in Section IV.

II. HAMILTONIAN AND FORMALISM OF SEMICLASSICAL APPROXIMATION

In this study, we considered the ionic Hubbard model of a half-filled 2D $L \times L$ square lattice [14, 15]. Since the discovery of high-temperature cuprate superconductors, several studies have been conducted on the 2D Hubbard model of a square lattice. In addition, the results of the Hubbard model of a 2D $L \times L$ square lattice with half-filled particle-hole symmetry are well understood. Therefore, we believe that this model is a useful benchmark for examining novel method.

The Hamiltonian of the ionic Hubbard model is expressed as

$$H = -t \sum_{i \in A, j \in B, \sigma} (c_{i\sigma}^\dagger c_{j\sigma} + \text{h.c.}) - \Delta \sum_{i \in A} n_i + \Delta \sum_{i \in B} n_i + U \sum_i n_{i\uparrow} n_{i\downarrow} - \mu \sum_{i\sigma} n_i, \quad (1)$$

where t , μ and U are the nearest-neighbor hopping, chemical potential and repulsive Coulomb interactions, respectively. Here, $c_{i\sigma}^\dagger$ and $c_{i\sigma}$ are the electron creation and annihilation operators at site i with spin σ , respectively. Δ is the ionic staggered potential that alternates sign between sites in sublattices A or B . In this study we considered only the half-filled case. The energy scale t was set to $t = 1$, and the size N_c of the noninteracting Hamiltonian with $U/t = 0$ was $N_c = L^2$.

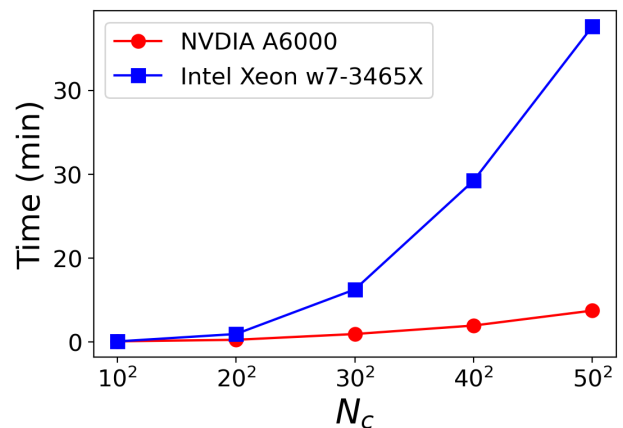


FIG. 2. (Color online) Computing time (min) as a function of N_c on CPU (Intel Xeon w7-3465X) and GPU (single NVIDIA RTX-6000A) to determine optimal $|\phi|$ in the Hubbard model on 2D $L \times L$ square lattice. N_c is defined as $N_c = L^2$.

Here, we present the formalism of the SCA approach. The partition function of the Hubbard model is expressed as

$$Z = \int D[c^\dagger, c] \exp[-S_{\text{eff}}]. \quad (2)$$

Here, the effective action can be written as

$$S_{\text{eff}} = \int_0^\beta d\tau \int_0^\beta d\tau' c^\dagger(\tau) \hat{a}(\tau - \tau') c(\tau') + U \int_0^\beta d\tau n_\uparrow(\tau) n_\downarrow(\tau), \quad (3)$$

where c^\dagger and c are the Grassmann variables, $c^\dagger = (c_\uparrow^\dagger, c_\downarrow^\dagger)^T$ and $c = (c_\uparrow, c_\downarrow)^T$. $\hat{a}(\tau - \tau')$ denotes the inversion matrix of $2N_c \times 2N_c$ Hamiltonian. β denotes the inverse temperature T . $n_\uparrow(\tau) n_\downarrow(\tau)$ are transformed into

$$n_\uparrow(\tau) n_\downarrow(\tau) = \frac{1}{4} (N(\tau)^2 - M(\tau)^2), \quad (4)$$

where $N(\tau) = n_\uparrow(\tau) + n_\downarrow(\tau)$ and $M(\tau) = n_\uparrow(\tau) - n_\downarrow(\tau)$ mean the charge and spin fluctuations, respectively. The SCA approach ignores the charge fluctuations $N(\tau)$.

The Gaussian form of the approximated partition function is derived via the Hubbard-Stratonovich transformation of the spin fluctuation term $M(\tau)$. The partition function can be rewritten as

$$Z = \int \int D[c^\dagger c] \int_{-\infty}^{\infty} d\phi e^{-H(\phi)}, \quad (5)$$

where $H(\phi) = -\frac{\beta\phi^2}{4U} + \int d\tau \int d\tau' c^\dagger(\tau) (\hat{a}(\tau\tau') + \frac{1}{2}\phi\sigma_z\delta(\tau - \tau')) c(\tau')$. σ_z is the Pauli matrix of z -component. All τ -dependent auxiliary fields $\phi_j(\tau)$ are approximated into static $\phi_j(\tau) = \phi_j$ without τ -dependence. After Fourier transformation and Grassmann integration of the partition function given in Eq. (5), the final partition function of the SCA is given by

$$Z = \int_{-\infty}^{\infty} d\phi_1 \dots \phi_{N_c} e^{-\beta V(\phi)}, \quad (6)$$

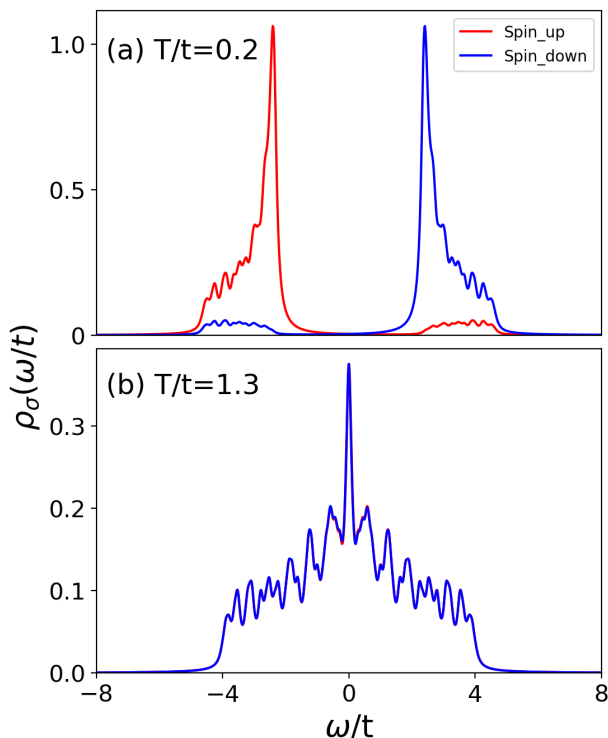


FIG. 3. (Color online) Density of states $\rho_\sigma(\omega/t)$ as a function of real frequency ω/t at spin σ in the Hubbard model on half-filled 2D 20×20 square lattice at $U/t = 6.0$ for (a) $T/t = 0.2$ and (b) 1.3.

where $V(\phi)$ denotes the potential generated by SCA. The detailed $V(\phi)$ is expressed as follows:

$$V(\phi) = \frac{1}{4U} \sum_j^{N_c} \phi_j^2 - T \sum_{\omega_n} \ln \det[-\beta(\hat{a}(\omega_n) + \wedge(\phi))], \quad (7)$$

where $\hat{a}(\omega_n)$ and $\wedge(\phi) = \text{diag}(\phi_1\sigma_z, \dots, \phi_N\sigma_z)$ are $2N_c \times 2N_c$ matrices. The Matsubara frequencies ω_n are represented by $\omega_n = (2n+1)\pi T$. The ϕ values with the lowest possible energy of $V(\phi)$ were computed using an ADAM optimizer based on the PyTorch library. Here, ϕ is the AF order parameter in SCA approach. After determining all ϕ , we modify H into an approximated $2N_c \times 2N_c$ Hamiltonian H_{SCA} with ϕ . $\rho(\omega)$ is determined as follows:

$$\rho_\sigma(\omega) = -\frac{1}{\pi} \text{Im} \left(\frac{1}{\omega + i\eta + \mu - H_{\text{SCA}}} \right), \quad (8)$$

where η denotes the broadening factor.

III. RESULT

First, we discuss the computation of Eq. (7) to confirm a feasible computation time. Computing the determinant of the $2N_c \times 2N_c$ matrix in Eq. (7) requires iterations of infinite ω_n values, which is not feasible. However, the high-frequency parts of ω_n are less important

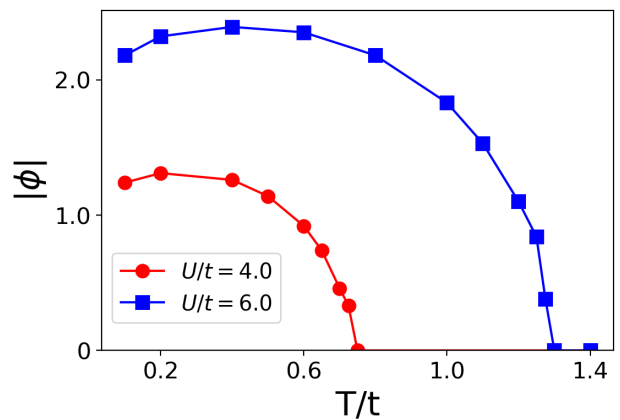


FIG. 4. (Color online) $|\phi|$ as a function of T/t in the Hubbard model on half-filled 2D 20×20 square lattice for $U/t = 4.0$ and 6.0.

for determining the exact AF order parameter $|\phi|$ within the approximation. Thus, we computed $|\phi|$ as a function of $\omega_{n_{\text{max}}}$; here, $\omega_{n_{\text{max}}}$ is the maximum Matsubara value considered in the determinant computation in Eq. (7). Fig. 1 shows AF order parameter $|\phi|$ as a function of $\omega_{n_{\text{max}}}$ for the Hubbard model with $T/t = 0.1$ and 0.6. $|\phi|$ increases with increasing $\omega_{n_{\text{max}}}$ and nearly converges at $\omega_{n_{\text{max}}} = 100$ in both the cases. Although ϕ is related to the gap size in the AF insulator, it does not affect the physical phase. We believe that it is sufficient to set $\omega_{n_{\text{max}}} = 100$ to reduce the computational burden on the results shown in Fig. 1.

Next, we discuss the computational expenses and limitations in the system size for the CPU and GPU. The computation of the determinant of the $2N_c \times 2N_c$ matrix via iteration of ω_n and the optimization to determine $|\phi|$, which has the lowest possible energy in $V(\phi)$ in Eq. (7), are the most computationally intensive steps; here, Eq. (7) includes loops, matrix determinant calculations, and optimizations of potential. The program was solved using the ADAM optimizer with an auto-gradient approach based on the Pytorch library. Fig. 2 shows the computation time as a function of N_c (associated hardware: an Intel Xeon w7-3465X CPU and a single NVIDIA RTX-A6000 GPU). Because the GPU first frees up memory space for parallel computation, a single GPU can count up to $N_c = 60^2$ for Matsubara frequency $n = 15$ in Eq. (7) with slowly increasing computing time, as shown in Fig. 2. However, the computational costs of the CPU in Eq. (7) polynomially increases with the increasing number of ϕ , even though the CPU can calculate significantly large sizes compared to a GPU.

We evaluated $\rho_\sigma(\omega/t)$ and $|\phi|$ of the pure Hubbard model without Δ/t for a half-filled 2D $L \times L$ square lattice with $L = 20$. Figs. 2 (a) and (b) show $\rho_\sigma(\omega/t)$ as a function of the real frequency ω/t at $U/t = 6.0$ for $T/t = 0.2$ and 1.3. Evidently, the AF insulator with a gap exhibits a low $T/t = 0.2$ in Figs. 3(a), because of the

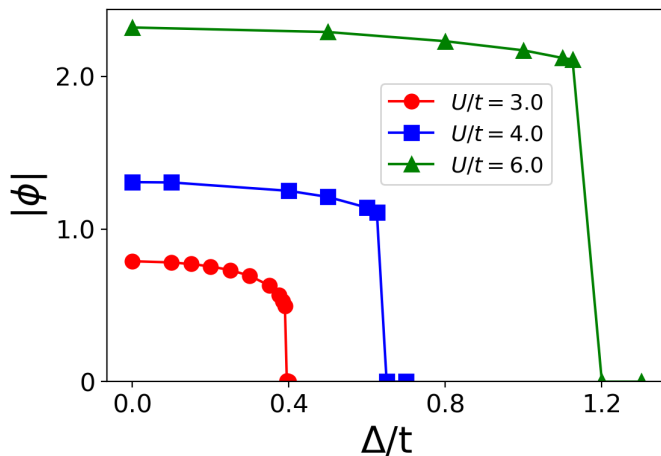


FIG. 5. (Color online) $|\phi|$ as a function of Δ/t for $U/t = 2.0$, 4.0 , and 6.0 in the half-filled ionic Hubbard model on $2D$ 20×20 square lattice at $T/t = 0.1$.

broken spin symmetry. The paramagnetic metal with van Hove peak at the Fermi level ($\omega/t = 0.0$) are shown at a high $T/t = 1.3$ in Figs. 3(b). We also show $|\phi|$ as a function of T/t for several U/t values in Fig. 4. An AF insulator with a finite $|\phi|$ is shown at low T for all U/t . The Neel T/t that eliminates $|\phi|$ in the AF order increases with U/t . The result does not show the Mott insulator at high T/t in strong interaction U/t and is similar to that obtained using the Hartree-Fock approximation because the SCA ignores charge fluctuations. However, the SCA based results are slightly better than those obtained using the Hartree-Fock approximation, because dynamical fluctuations are considered at the zero Matsubara frequency level for the static imaginary time τ beyond the Hartree-Fock approximation.

Finally, we investigated the ionic Hubbard model, which displays a charge density wave (CDW), an AF insulator, and a metal. Fig. 5 shows $|\phi|$ as a function of Δ/t for $U/t = 2.0$, 4.0 , and 6.0 in the half-filled ionic Hubbard model on $2D$ 20×20 square lattice at $T/t = 0.1$. Evidently, $|\phi|$ gradually decreases around the critical ionic potential $\Delta^*/t = 0.39$ for $U/t = 3.0$, whereas it shows an abrupt decrease at $\Delta^*/t = 0.68$ and 1.19 for $U/t = 4.0$ and 5.0 , respectively. We estimate that the gently falling shape around $\Delta^*/t = 0.39$ of $U/t = 3.0$ can be attributed to the presence of the metallic state between the CDW and AF insulators. As U/t increases, the gently dropping curve suddenly shows an abrupt drop at Δ^*/t . This change in the curve indicates the absence of metallic state between the CDW and AF insulators. In order to confirm the presence of metallic state in weak interaction region of $U/t = 3.0$, we plotted $\rho_\sigma(\omega/t)$ at $U/t = 3.0$ and $T/t = 0.1$ for $\Delta/t = 0.3$, 0.39 and 0.4 in Figs. 6(a), (b) and (c), respectively. A gap opening in $\rho_\sigma(\omega/t)$ is broken by the spin symmetry in weak Δ/t of Fig. 6(a), while it is induced by broken periodic potential in strong Δ/t of Fig. 6(c). Two different phases in Figs. 6(a) and (c) mean

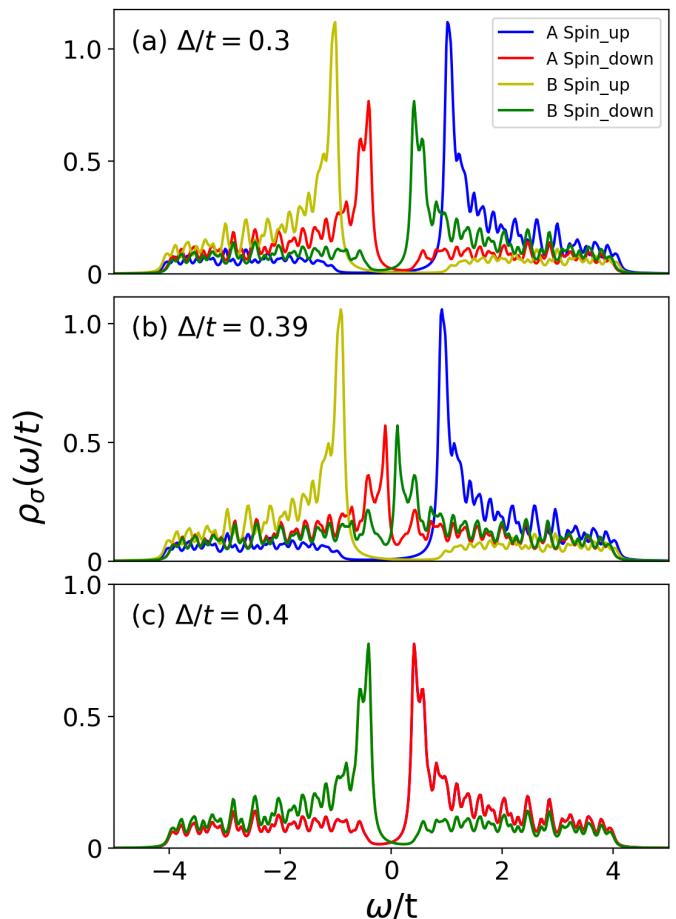


FIG. 6. (Color online) $\rho_\sigma(\omega/t)$ as a function of real frequency ω/t in the ionic Hubbard model on $2D$ 20×20 square lattice at $U/t = 3.0$ and $T/t = 0.1$ for (a) $\Delta/t = 0.3$, (b) 0.39 and (c) 0.4 .

the AF insulator and CDW, respectively. We confirmed the AF metal with broken spin symmetry and finite density at Fermi level in intermediate region of Fig. 6(b).

IV. CONCLUSION

The Hubbard model of a $2D$ $L \times L$ square lattice is an unsolved problem in physics. Exact numerical methods, such as ED and QMC, are limited by the size of the $2D$ lattice. Therefore, developing approximate methods to compute the physical properties of large-scale lattice sizes is necessary. In this study, we developed the SCA+ADAM approach to compute $\rho_\sigma(\omega/t)$ and $|\phi|$ of a $2D$ ionic Hubbard model with long-range spatial correlations within an appropriate computational duration. We evaluated the computation time as a function of the lattice size on the CPU and GPU as well as examined the physical properties of the Hubbard model without ionic potential and compare them with the results computed using the Hartree-Fock approximation method. Finally,

the one-particle properties and AF order parameter of the ionic Hubbard model were analyzed.

Notably, the disordered Hubbard model, which is characterized by a random onsite potential and is more interesting and complex than the ionic Hubbard model, requires a large lattice to capture the competition between electron hopping, random onsite potentials, and Coulomb interactions [16]. The SCA+ADAM approach can be used to compute the physical properties of the Hubbard model with competition between long-range spatial AF correlations and onsite random potential. Therefore, we believe that the proposed method can be applied to the

disordered Hubbard model and other such fundamental physical problems in the future.

V. ACKNOWLEDGEMENTS

This work was supported by Ministry of Science through NRF-2021R1111A2057259 funded by the Korean government. We would like to acknowledge the hospitality at APCTP where part of this work was done.

-
- [1] M. Imada, A. Fujimori, *Rev. Mod. Phys.* **70**, 1039 (1998).
 - [2] Y. Ohta, K. Tsutsui, W. Koshibae, and S. Maekawa, *Phys. Rev. B* **50**, 13594 (1994).
 - [3] A. Go and A. J. Millis, *Phys. Rev. B* **96**, 085139 (2017).
 - [4] J.E. Hirsch and R.M. Fye, *Phys. Rev. Lett.* **56**, 2521 (1986).
 - [5] E. Gull, A. J. Millis, A. I. Lichtenstein, A. N. Rubtsov, M. Troyer, P. Werner, *Rev. Mod. Phys.* **83**, 349 (2011).
 - [6] A. Georges, G. Kotliar, W. Krauth, and M. Rozenberg, *Rev. Mod. Phys.* **68**, 13 (1996).
 - [7] F. Evers and A. D. Mirlin, *Rev. Mod. Phys.* **80**, 1355 (2008).
 - [8] S. Moukouri and M. Jarrell, *Phys. Rev. Lett.* **87**, 167010 (2001).
 - [9] B. Kyung and J.S. Tremblay, *Phys. Rev. Lett.* **90**, 099702 (2003).
 - [10] T. Maier, M. Jarrell, T. Pruschke, M. H. Hettler, *Rev. Mod. Phys.* **77**, 1027 (2005).
 - [11] S. Okamoto, A. Fuhrmann, A. Comanac, and A. J. Millis, *Phys. Rev. B* **71**, 235113 (2005).
 - [12] H. Lee, Y.-Z. Zhang, H. Lee, Y. Kwon, H. O. Jeschke, R. Valenti, *Phys. Rev. B* **88**, 165126 (2013).
 - [13] K. Diederik and B. Jimmy, arXiv:1412.6980 (2014).
 - [14] K. Bouadim, N. Paris, F. Hébert, G. G. Batrouni, and R. T. Scalettar *Phys. Rev. B* **76**, 085112 (2007).
 - [15] A. Go and G. S. Jeon, *Phys. Rev. B* **84**, 195102 (2011).
 - [16] P. W. Anderson, *Phys. Rev.* **109**, 1492 (1958).